
# Memo 115

## Focal Plane Array Simulations with MeqTrees 1:Beamforming

A.G. Willis

B.Veidt

A. Gray

08/09

# Focal Plane Array Simulations with MeqTrees 1:Beamforming

A.G. Willis, B. Veidt and A. Gray
National Research Council of Canada
Dominion Radio Astrophysical Observatory
Penticton, BC, Canada V2A 6J9
*tony.willis@nrc-cnrc.gc.ca*

August 26, 2009

## 1 Introduction

For centimetre-wave radio astronomy, the key science problems [1] over the next several decades will require not only observations at very high sensitivity, but also wide fields so that large areas of the sky can be surveyed. It is expected that the required field-of-view (FoV) will be on the order of 20 square degrees [2]. This means that future telescopes, such as the Square Kilometre Array (SKA) [3] cannot simply be reproductions of existing telescopes (such as the Very Large Array or Westerbork Synthesis Radio Telescope) which have single feeds at the focus of each reflector antenna and thus a narrow field-of-view. New technologies and techniques will be required to enable this expansion of FoV at a reasonable cost. We will first examine FoV expansion using conventional technology (feed horn clusters) and then introduce a new technology that uses a phased array to sample the focal fields of a reflector antenna and then synthesize the desired telescope response with a beamforming network.

Arrays of horn antennas feeding reflector antennas have been used for many years for communications applications. For example, the antennas on geostationary communication satellites produce a tight cluster of beams that only illuminate the regions of the globe that the communications provider is licensed to serve [4]. The main deficiency in these systems from an astronomy point-of-view is that the spacing of the horn antennas is not small enough for Nyquist sampling of the sky. For satellite operators this results in a ripple in signal power across the coverage area ($\sim 20 - 30\%$) which can be accommodated by a small change in ground station antenna size or in increase in transmitter power. For astronomers the result is a loss of spatial frequency information which requires additional observations at slightly different directions to recover.

Horn clusters have been used on centimetre- and millimetre-wave single-dish radio telescopes. A notable example is the Parkes Multibeam Receiver [5] which provides 13 beams on the Parkes radio telescope. This receiver operates between 1.27 and 1.47 GHz, a 16% bandwidth. Although efforts were taken to design the feed horns for dense packing, the beams are spaced twice the half-power width (2 x FWHM) apart, again exceeding what is required for Nyquist sampling. This problem can be understood as a result of the array of horns being unable to adequately sample fields in the focal plane. This is not only due to gaps between the horns but more significantly because the field amplitude across the radiating aperture of each horn is tapered to a low value at the outside edge, so that the effective area of each horn is less than the actual physical area.

Future telescopes will have an instantaneous observing bandwidth of an octave or more. This creates another problem for horn clusters. Consider the "Eleven Antenna" [6] which radiates from the whole aperture at low frequencies and only the central portion at high frequencies. This behavior would be the same for *any* wide-band antenna with an illumination pattern that is constant with frequency. An array constructed with a wide-band feed antenna would have the element spacing determined by the lowest operating frequency which sets the diameter of the aperture. The key point to note is that the size of the radiating aperture decreases with increasing frequency while the element spacing is fixed, resulting in a decrease of sampling efficiency of the focal plane.

An alternative to an array of horns is an array of simple densely-packed antenna elements. These low-gain antenna elements sample the focal fields. After amplification, filtering, frequency conversion and digitization, the signals are combined in a beamformer to synthesize beams with desired characteristics. Unlike horn arrays which have a single horn per beam, the outputs of several tens of elements are combined to synthesize a single beam. Another difference is that the synthesized beams can be placed as close together as desired (and overlap) since the amplified and digitized signals can be routed to any number of beamformers.

A leading candidate for element geometry is the tapered-slot antenna [7], also known as the Vivaldi antenna [8]. An example of Vivaldi elements in an array is shown the upper photo of Fig. 1. This element consists of a metal plane with a narrow slot which expands in width as it nears the end of the element. Coupling to a low-noise amplifier occurs in narrow part of the slotline and coupling to the radiation field occurs in the flared region. This is a non-resonant traveling-wave antenna and this allows the elements to be packed very densely with spacings between $\lambda/10$ and $\lambda/2$ (resonant antennas are detuned for element separation less than $\sim \lambda/2$). Such close spacing is crucial for preventing the appearance of grating lobes which would point beyond the edge of the reflector antenna and strike the ground, increasing the spillover noise contribution to the system temperature. A typical radiation pattern is shown in the bottom diagram of Fig. 1. Although element radiation patterns will over-illuminate most reflector antennas, the weighted sum of the outputs of several elements in a beamformer will suppress spillover radiation and enhance coupling to the reflector. (Note that beamforming cannot selectively suppress grating lobes in a similar way.) An important characteristic of Vivaldi arrays is that they have a large bandwidth of an octave or more (measured by the variation in terminal impedance with frequency and by the variation in radiation pattern with frequency).

Once we have an array that can sample the focal fields, the next crucial component in the system is the beamformer and the weights and calibration methods used to program it. The primary goal of the beamformer is to optimally illuminate the reflector. Other operations can be performed by appropriate control of beamformer coefficients:

- suppress cross polarization response over the field-of-view of the feed,
- electronically de-rotate the observed field for telescopes using an alt-az mount,
- suppress interference.

Accurate calibration and correction of the instrumental polarization response will be important for SKA wide-field surveys as "The Origin and Evolution of Cosmic Magnetism" is one of the five "key science projects" planned for the SKA [9]. Radio waves are powerful probes of cosmic magnetic fields: non-thermal synchrotron radiation radiation is proportional to the strength of the field, the degree of polarization gives us information about the ordering of the field while the position angle of the polarized emission tells us the orientation of the field in the sky plane. Faraday rotation provides us with information about the strength of the field along the line of sight. The Zeeman effect provides an independent measure of field strength in cold gas clouds. One of the goals of the SKA is to do an all-sky survey of rotation measures. Such a rotation measure survey would be a powerful probe for studying foreground magnetic fields at all redshifts. Wide-field imaging projects involving polarimetry of faint radio sources are revealing new astrophysical phenomena such as those described in [10].

In order to get a survey such as the rotation measure survey mentioned previously completed in a reasonable amount of time, one current design for the SKA at centimeter wavelengths is a collection of 10 to 15 metre parabolic antennas equipped with phased-array focal plane array receiver systems.

Although a number of pioneering phased-array Focal Plane array systems have been simulated [11] or are being built ([12], [13],[14],[15]), the emphasis so far has been from the engineering viewpoint. Here we examine such systems from the viewpoint of doing astronomical surveys with such arrays and we look at some of the calibration and data correction issues which will have to be addressed in order to obtain high quality wide-field polarization data.

The understanding of how instrumental polarization and other radio telescope instrumental responses affect observed data was put into its current perspective through the introduction of what is now called the Measurement Equation [16]. We give a brief review of the Measurement Equation and show how it can be applied to focal plane array simulations in the next section.

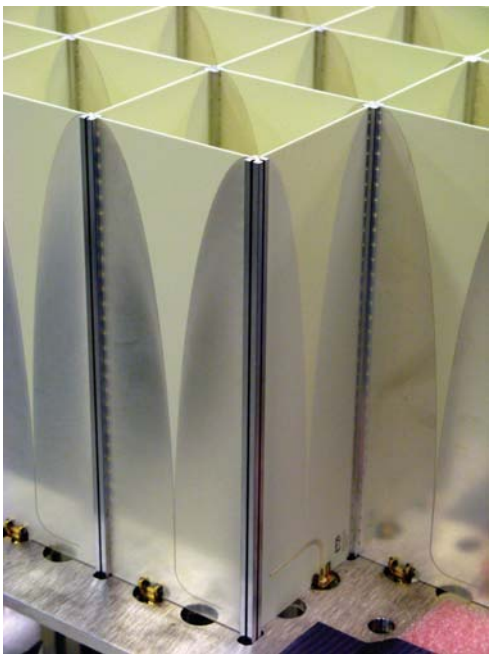

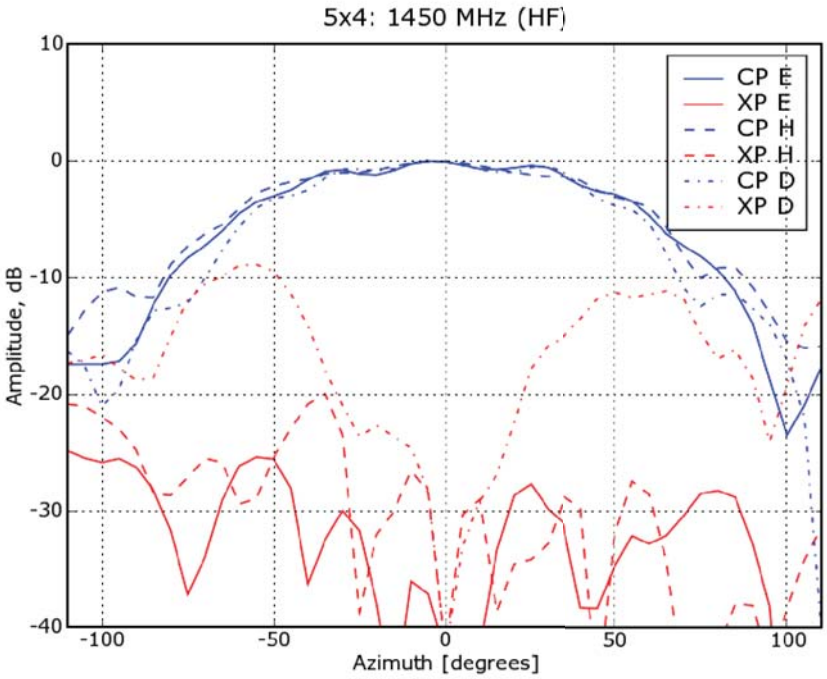


Figure 1: The top photograph shows a close-up of Vivaldi elements in an array. Each element is constructed of microwave printed-circuit board material and is $\lambda/2$ wide at the highest operating frequency. Electrical connection between elements is provided by the metal posts with mounting slots. The bottom figure shows radiation patterns for a single Vivaldi element near the centre of a large array. This plot shows the co- (CP) and cross-polarized (XP) responses in three cuts: E (coplanar with the Vivaldi element circuit board), H (plane perpendicular to the E plane) and D (plane at 45°to E plane).

# 2 Radio telescope Simulations using the Measurement Equation

The exact measurement of cosmic radio source properties is hampered by instrumental effects, which must be understood and removed before one can use the data for scientific analysis. In order to obtain high angular resolution, most modern radio telescopes are composed of collections of radio interferometers. The understanding of instrumental effects associated with radio interferometers was put into its current perspective through the introduction of what is now called the Measurement Equation [16].

## 2.1 Jones Matrices

The Measurement Equation says that the instrumental effects associated with an interferometer, which are not necessarily limited to polarization effects, can be described by a sequence of two $2 \times 2$ *station*-based response matrices, called 'Jones matrices'. Each Jones matrix describes a corrupting influence on the incoming radio waves. Jones matrices that model 'image-plane' effects depend on the source position (direction) $\vec{\rho}$. Some also depend on the antenna position $\vec{r}_\mathsf{i}$. Many of them may depend on time and frequency as well. Aips++ Note 185 [17] gives a detailed discussion of individual Jones matrices. The notation used here is derived from that of Aips++ Note 185.

The $2 \times 2$ Jones matrix $\mathsf{J_i}$ for *station* $\mathsf{i}$ can be decomposed into a product of several $2 \times 2$ Jones matrices, each of which models a specific *station*-based instrumental effect in the signal path. Here we are concerned with the following sequence of Jones matrices:

$$\mathsf{J_i} \;=\; \mathsf{G_i}\;\mathsf{D_i}\;\mathsf{E_i}\;\mathsf{P_i}\;\mathsf{K_i} \tag{1}$$

where

| | |
|---|---|
| $\mathsf{K_i}(\vec{\rho}.\vec{r}_\mathsf{i})$ | factored Fourier Transform kernel, |
| $\mathsf{P_i}$ | projected *receptor* orientation(s) w.r.t. the sky, |
| $\mathsf{E_i}(\vec{\rho})$ | voltage primary beam, |
| $\mathsf{D_i}$ | position-independent *receptor* cross-leakage, |
| $\mathsf{G_i}$ | electronic complex gain (*feed*-based contributions only). |

Additional Jones matrices can be used to model, for example, ionospheric and tropospheric behaviour, but they are not used in the simulations described here. The result is evaluated by a sequence of 2 x 2 matrix multiplications going from left to right through the sequence of Jones matrices. See Smirnov's [18] MeqTrees workshop presentations for a detailed description of this procedure.

The Jones matrices may be viewed as forming a transformation matrix between a Stokes coherency vector, or matrix, and the observed visibilities [16], [19]. The visibility for an interferometer composed of *station* $\mathsf{i}$ and *station* $\mathsf{j}$ is then given by the following equation, where $\vec{V}_\mathsf{ij}$ is the visibility, $\vec{I}$ is the incoming electromagnetic coherency matrix, and $\mathsf{J}_\mathsf{j}^*$ is the transposed complex conjugate of $\mathsf{J_j}$:

$$\vec{V}_\mathsf{ij} \;\equiv\; \begin{pmatrix} \mathsf{v_{ip\,jp}} & \mathsf{v_{ip\,jq}} \\ \mathsf{v_{iq\,jp}} & \mathsf{v_{iq\,jq}} \end{pmatrix} \;=\; \mathsf{J_i}\;\vec{I}\;\mathsf{J}_\mathsf{j}^* \tag{2}$$

The subscripts $\mathsf{i}$ and $\mathsf{j}$ are the labels of the two *feed*s that make up the *interferometer*. The subscripts $\mathsf{p}$ and $\mathsf{q}$ are the labels of the two output *IF-channel*s from each *feed*. For linear polarization

$$\vec{I} \;=\; 0.5 \begin{pmatrix} I+Q & U+iV \\ U-iV & I-Q \end{pmatrix} \tag{3}$$

and for circular polarization

$$\vec{I} \;=\; 0.5 \begin{pmatrix} I+V & Q+iU \\ Q-iU & I-V \end{pmatrix}.$$

## 2.2 Simplifying Assumptions

For the simulations presented here, some simplifying assumptions are initially made:

- The $\mathsf{D_i}$ Jones matrix refers to position-independent *receptor* cross-leakage. It is generally associated with various internal interactions with an antenna feed [20]. Although it is expected that there will be considerable position-independent cross-leakage issues with actual phased array feeds, our main focus in this paper is the behaviour of position dependent cross-leakage. Since these terms are contained within the off-diagonal terms of the E-Jones matrix, we will assume that the D-Jones matrix is a unit diagonal matrix and ignore any actual D-Jones contribution for the remainder of this paper. (For those interested, Cotton[21] provides a good overview of methods used to calibrated the D-Jones terms in actual synthesis arrays.)

- As we are not modeling the instrument's Fourier response to sources in the field, we set $\mathsf{K_i}$ to unit diagonal matrix.

- We use perfectly calibrated gains, so $\mathsf{G_i}$ also becomes a unit diagonal matrix.

- $\mathsf{P_i}$ is the projection matrix, which models the *projected* orientation of the *receptor*s with respect to the electrical frame on the sky. For properly aligned linearly polarized feeds this may be reduced to

$$\mathsf{P_i^+} \;=\; \begin{pmatrix} \cos\beta & -\sin\beta \\ \sin\beta & \cos\beta \end{pmatrix}$$

  where $\beta$ is the parallactic angle. This is a unit diagonal matrix for the case where the receptors are aligned perfectly with the East and North (L and M) axes for equatorially mounted dishes, and for azimuth-elevation telescopes at transit. We consider such a case here.

- The Measurement Equation does not require that the individual antennas of a baseline pair be identical: in fact, one of its strengths is that it can describe the coupled interferometer responses of heterogeneous antennas. However, for these simulations we assume homogeneity of the array.

We will consider the effects of time varying $\mathsf{G_i}$ and $\mathsf{P_i}$ terms in future memos.

## 2.3 E-Jones and Instrumental Polarization

From Equations 1 and 2 and the assumptions above, we see that the expected behavior of the primary beam total intensity or power pattern associated with *station* i and *station* j can now be obtained simply with

$$\vec{V}_{\mathsf{ij}}(\vec{\rho}) \;=\; \mathsf{E_i}(\vec{\rho})\;\vec{I}\;\mathsf{E_j}(\vec{\rho})^* \tag{4}$$

We now simulate how the E-Jones matrices add instrumental polarization to the observed visibilities. We can do this by using an unpolarized coherency matrix with unit signal:

$$\vec{I} \;=\; 0.5\begin{pmatrix} 1 & 0 \\ 0 & 1 \end{pmatrix} \tag{5}$$

The position-dependent primary beam attenuation and the *position-dependent* leakage is given by the E-Jones matrix:

$$\mathsf{E_i^+}(\vec{\rho}) \;=\; \mathsf{E_i^\odot}(\vec{\rho}) \;=\; \mathsf{E_i}(\vec{\rho}) \;=\begin{pmatrix} \mathsf{e_{ipp}}(\vec{\rho}) & \mathsf{e_{ipq}}(\vec{\rho}) \\ \mathsf{e_{iqp}}(\vec{\rho}) & \mathsf{e_{iqq}}(\vec{\rho}) \end{pmatrix} \tag{6}$$

Here, the position-dependent components of the E-Jones matrix are the complex-valued voltage responses of an individual antenna in an interferometer pair, known from measurements or simulations (see, for example, Figure 2).

The subscript convention is as follows: $\mathsf{e_{ipq}}$ is an element of matrix $\mathsf{Y}$ for *antenna* i, which models the 'coupling factor' for the signal going *from receptor* q *to* output *IF-channel* p. So $\mathsf{e_{ipp}}$ describes a co-polarization response, while $\mathsf{e_{ipq}}$ describes a cross-polarization, or leakage, response.

From Equations 4, and 5, and 6 we find the observed visibilities to be:

$$\begin{pmatrix} \mathsf{v_{ip\,jp}}(\vec{\rho}) & \mathsf{v_{ip\,jq}}(\vec{\rho}) \\ \mathsf{v_{iq\,jp}}(\vec{\rho}) & \mathsf{v_{iq\,jq}}(\vec{\rho}) \end{pmatrix} \;=\; \begin{pmatrix} \mathsf{e_{ipp}}(\vec{\rho}) & \mathsf{e_{ipq}}(\vec{\rho}) \\ \mathsf{e_{iqp}}(\vec{\rho}) & \mathsf{e_{iqq}}(\vec{\rho}) \end{pmatrix} \begin{pmatrix} 0.5 & 0 \\ 0 & 0.5 \end{pmatrix} \begin{pmatrix} \mathsf{e_{jpp}}(\vec{\rho})^* & \mathsf{e_{jqp}}(\vec{\rho})^* \\ \mathsf{e_{jpq}}(\vec{\rho})^* & \mathsf{e_{jqq}}(\vec{\rho})^* \end{pmatrix} \tag{7}$$

Since we have not used any Fourier transform kernel in this equation the individual components in the $V$ matrix describe the total intensity responses of the instrument including the instrumental Stokes parameter.

For the case of linear polarization we know (from Equation 3) that:

$$\begin{pmatrix} \mathsf{v}_{\mathsf{ip\,jp}}(\vec{\rho}) & \mathsf{v}_{\mathsf{ip\,jq}}(\vec{\rho}) \\ \mathsf{v}_{\mathsf{iq\,jp}}(\vec{\rho}) & \mathsf{v}_{\mathsf{iq\,jq}}(\vec{\rho}) \end{pmatrix} = 0.5 \begin{pmatrix} \hat{I}(\vec{\rho}) + \hat{Q}(\vec{\rho}) & \hat{U}(\vec{\rho}) + i\hat{V}(\vec{\rho}) \\ \hat{U}(\vec{\rho}) - i\hat{V}(\vec{\rho}) & \hat{I}(\vec{\rho}) - \hat{Q}(\vec{\rho}) \end{pmatrix} \tag{8}$$

where $\hat{I}$, $\hat{Q}$, $\hat{U}$, and $\hat{V}$ are the observed (i.e., uncorrected) Stokes parameters. Rearranging terms we end up with:

$$\hat{I}(\vec{\rho}) = \mathsf{v}_{\mathsf{ip\,jp}}(\vec{\rho}) + \mathsf{v}_{\mathsf{iq\,jq}}(\vec{\rho}) \tag{9}$$

$$\hat{Q}(\vec{\rho}) = \mathsf{v}_{\mathsf{ip\,jp}}(\vec{\rho}) - \mathsf{v}_{\mathsf{iq\,jq}}(\vec{\rho}) \tag{10}$$

$$\hat{U}(\vec{\rho}) = \mathsf{v}_{\mathsf{iq\,jp}}(\vec{\rho}) + \mathsf{v}_{\mathsf{ip\,jq}}(\vec{\rho}) \tag{11}$$

$$\hat{V}(\vec{\rho}) = i(\mathsf{v}_{\mathsf{iq\,jp}}(\vec{\rho}) - \mathsf{v}_{\mathsf{ip\,jq}}(\vec{\rho})) \tag{12}$$

These four equations gives us the interferometer's direction-dependent responses in Stokes $I$, $Q$, $U$, and $V$. A similar result can be obtained for receptors sensitive to circular polarization.

### 2.4 Application to Phased-Array Feeds

To simulate the sky response, $\mathsf{e}_{\mathsf{ipq}}(\vec{\rho})$, of a focal plane array that is phased up in a particular direction on *antenna* $\mathsf{i}$ we must use appropriate complex-valued weights for the $n$ E-Jones matrices that describe the $n$ individual feed elements on *antenna* $\mathsf{i}$:

$$\mathsf{e}_{\mathsf{ipq}}(\vec{\rho}) = \frac{\sum_n w_{in}\ \mathsf{e}^n_{\mathsf{ipq}}(\vec{\rho})}{\sum_n w_{in}} \tag{13}$$

where $w_{in}$ is a complex-valued weight for the n-th element beam, $\mathsf{e}^n_{\mathsf{ipq}}(\vec{\rho})$, of the phased array elements on *antenna* $\mathsf{i}$. Some methods for setting these weights to form array beams are discussed below.

## 3 Experimental Setup

We designed a simulated focal plane array system placed at the prime focus of a parabolic dish with the GRASP antenna design package [22]. This software uses Physical Optics and Physical Theory of Diffraction to calculate currents induced on the reflector by feed antenna illumination, and from these currents the far-field radiation pattern is calculated. The basic simulation setup consisted of the following:

- Parabolic dish diameter = 10m; Focal length = 4.5m
- 90 dipole elements in each of X and Y directions. The layout is shown schematically in Fig. 2
- Frequency = 1500 MHz; Spacing = lambda / 2
- No coupling between elements; No feed struts in simulation

This dipole simulation is not something one would want to use for an actual antenna design. But the introduction of feed elements (dipoles) which can have a rather high instrumental polarization [20], allows us to examine how adjustment of the phased array weights can used to reduce the instrumental polarization. The GRASP package was used to calculate the element voltage parallel and cross-leakage voltage patterns on the sky for each of the 180 elements in the array. These voltage patterns correspond directly to the E-Jones matrices discussed earlier. Since GRASP can output the simulated antenna responses directly in L,M (direction cosine) coordinates, it was easy to translate the GRASP data into FITS files which could be read and processed by astronomy data reduction packages. The output of a GRASP calculation of the raw voltage response for the usual 'typical' dipole element for both the main and cross-leakage responses is shown in the bottom display of Fig. 2.

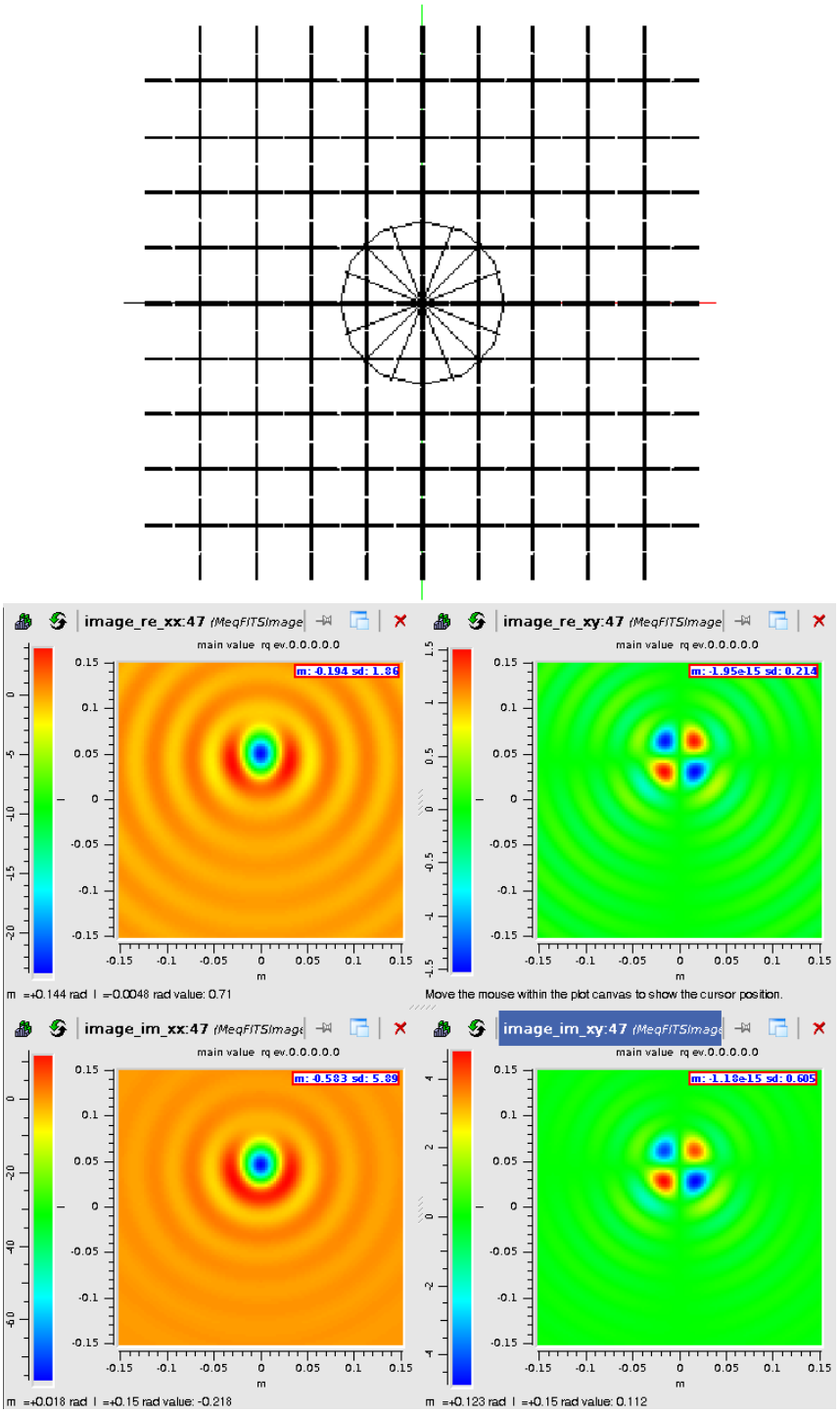


Figure 2: The upper diagram shows a simplified representation of the artificial Focal Plane dipole array used in GRASP simulations. The circle at the centre of the image shows the implied area that an individual 1500 MHz horn would require. The lower display shows a 'typical' off-boresight raw voltage pattern as calculated by GRASP. The left column shows the real and imaginary co-polarization response while the right column shows the real and imaginary cross-polarization (leakage) responses. The coordinates of the images are given in radians.

The sensitivity to an area on the sky as seen by the entire array is shown in Figure 3. This figure shows that our simulated array has a sensitivity within ten percent of the maximum out to a distance of about 0.06 radians or about 200 arcmin from the nominal field centre position). As the nominal FWHM of a phased up beam is about 75 arcmin (see below), we should be easily able to able to phase up at least a 5 x 5 array of independent beams on the sky. The results presented below support this conclusion.

### 3.1 Determining Beam Weights

MeqTrees[23] is a software simulation and calibration package designed for the explicit description of radio telescope behaviour in terms of Jones matrices. The default behaviour is to describe a Jones matrix in terms of its time and frequency behaviour. One can extend the domains to include up to five additional dimensions. So in addition to time and frequency dependent behaviour we can describe antenna responses as functions of the L and M direction cosines on the tangent plane of the sky. We produced FITS files from the E-Jones L,M responses produced by GRASP. These FITS files could be loaded into MeqTrees via the MeqTrees FITSImage node. Consequently we could use these E-Jones responses in various MeqTrees scripts to simulate telescope responses.

We used MeqTrees to derive focal plane array weights in a given direction in the sky as follows. Firstly we obtained phase-conjugate weights by interpolation of the beam voltage co-polarization responses to the exact L,M position where we wished to phase up the beam. The resulting total intensity response for a conjugate-weighted phased-up beam centred on boresight is shown at the top of Figure 4. The cross-sections through the beam illustrate that this particular phased-up beam has a high sidelobe structure which could lead to increased (and undesirable) responses to sources outside the main beam field of view.

However, MeqTrees can solve for optimized weights to fit any mathematical function or actual feed pattern that can be described on a two-dimensional L,M grid. We used the phase-conjugate weights as initial guesses for the MeqTrees solver, which then adjusts the values of these weights to obtain a best fit to the target function or beam. In the experiments described here we fitted the X and Y co-polarization voltage beams separately to the target patterns.

We used the resulting weights (Equation 18) to form a 'phased-up' E-Jones response for an antenna (Equation 9) and then created the expected primary beam pattern for an array composed of such antennas through use of equations 10 through 17.

The three rows in Figure 4 shows the results of taking the boresight phase-conjugate weights and fitting to three different patterns. The top row shows the results of a fit to a Gaussian with a HPBW of 75 arcmin (this value was obtained from the phase-conjugate weighted beam shown at the top of Figure 4). The middle row shows a fit to a prolate-spheriodal function with, again, a HPBW of approximately 75 arcmin. The bottom row shows the result of a fit to a single feed antenna pattern calculated with GRASP. We centred the feed at the focal point on boresight. The feed antenna illuminated the reflector with a linearly-polarized calculated Gaussian radiation pattern. At the edge of the dish the feed illumination had a taper of 12 dB relative to the centre of the beam. Simulation parameters of the dish were similar to what was used for the dipole FPA calculations and are:

- reflector diameter = 10m
- focal length = 4.5m
- frequency = 1.5 GHz
- edge taper of feed illumination = 12 dB
- blockage by the feed horn and scattering by feed support struts are not taken into account.

Note that although the simulated voltage response beams have various symmetries around the boresight (see also [11]) we did not make any assumptions about symmetry in our calculations as real-life phased-array beams do not have exact symmetries (See the ASTRON JIVE Daily Image for 27-03-2008)

An examination of Figure 4 shows that although the Gaussian and prolate fits lower the sidelobe responses significantly, there are residual differences with respect to the main beam shape. However we obtain an extremely good fit of both the main beam and sodelobes with respect to the GRASP-designed pattern as is

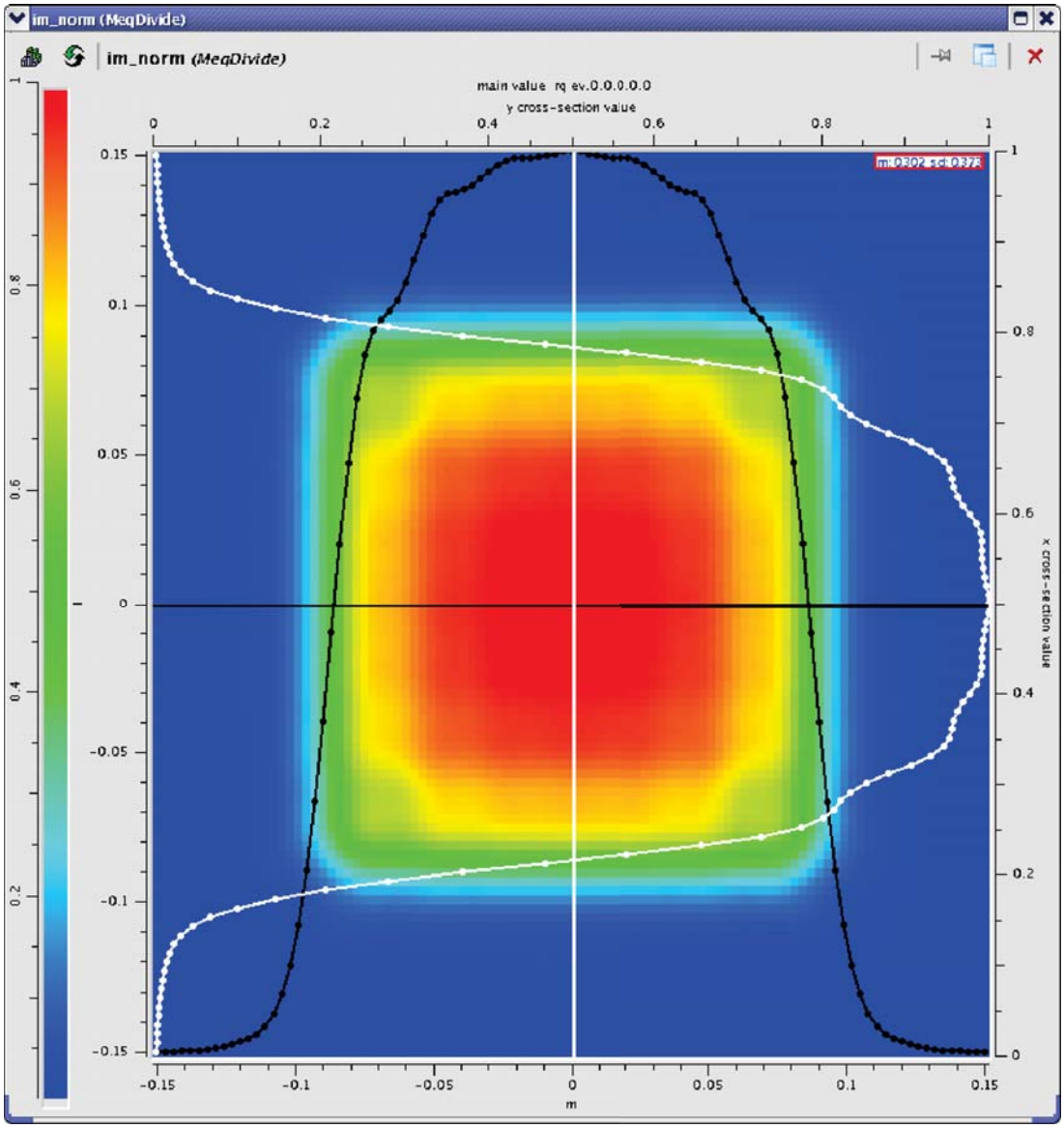


Figure 3: The illumination of the sky with the simulated focal plane array. We plot the summed power response as a function of position (L,M coordinates in radians) relative to boresight and normalized to a maximum of unity.

shown in the bottom row of this figure. The residuals are at most 0.002 over the whole field of view for this fit. Consequently, we use this GRASP design as the target pattern in the remainder of this memo.

Figures 5 though 8 show the Stokes I, Q, U and V response of phased up beams in increments of 1 x FWHM (75 arcmin) out to 2 x FWHM in L and M. The coordinates in each of the images give the offset from boresight in degrees. Each beam is centred in its frame but note the coordinate offsets. The conjugate weighted beams shown in the top half of Figure 5 have a reasonable resemblance to the measured phased-array beams given in the ASTRON JIVE Daily Image for 27-03-2008.

Note in Figure 6 how the fit to the GRASP design suppresses the instrumental Q response in comparison to the instrumental Q response present with conjugate weighting. Although the improvements are not as dramatic, the instrumental U and V responses (Figures 7 and 8) are also lowered slighly with the GRASP-target fitting.

Figures 9 though 16 show more detailed plots of the results of phasing up beams at boresight, and at offsets of 1, 2 and 3 times the nominal FWHM along the L axis with M set to zero. Each image shows the Stokes I response (shown on a logarithmic scale as we wish to emphasize the low level sidelobe responses) along with the instrumental Stokes Q, U and V responses, all of which are shown with a linear scale.

Note how the instrumental Q term is lower when we use the GRASP-target fits in contrast to the simpler phase-conjugate weighting scheme. This is perhaps not surprising as we are simulating a linearly polarized system and the instrumental Q is given by the difference of the co-polarization XX and YY responses, which we have tried to adjust to have the same shape.

The lower half of each diagram shows the distribution of weights for each element in the focal plane array, using a plotting scheme similar to that of Brisken and Craeye [11]). The amplitudes displayed are normalized to that of the maximum weight found for the field being studied.

# 4 Conclusions

We have developed a simulation procedure which shows that beam-forming techniques should be capable of improving the beam shape and lowering the instrumental polarization of phased array feed systems. We hope that actual feed systems developed for focal plane arrays have significantly less instrumental polarization than the simulated dipole system described here. However the techniques outlined here may also be of use in suppressing actual instrumental polarization to the lowest degree possible. This would help minimize post-observation data processing.

Further memos in this series will present some simulations for cases where the $\mathsf{G}_\mathsf{i}$ and $\mathsf{P}_\mathsf{i}$ Jones matrices may vary as a function of time, and for cases where it may be desirable to suppress the response of individual elements in the FPA.

# 5 Acknowledgments


- MeqTrees team - Oleg Smirnov, Sarod Yatawatta, Maaijke Mevius, Jan Noordam - for advice and assistance
- the referee for helpful comments


# References


[1] C. Carilli and S. Rawlings, Eds., *Science with the Square Kilometre Array*, ser. New Astronomy Reviews. Elsevier B.V., Dec. 2004, vol. 48. [Online]. Available: http://www.skatelescope.org/pages/page_sciencegen.htm

[2] R. T. Schilizzi, P. Alexander, J. M. Cordes, P. E. Dewdney, R. Ekers, A. J. Faulkner, B. M. Gaensler, P. J. Hall, J. L. Jonas, and K. L. Kellermann, "Preliminary specifications for the square kilometre array," International SKA Project Office, Tech. Rep., 2007. [Online]. Available: http://www.skatelescope.org/PDF/Preliminary_SKA_Specifications.pdf

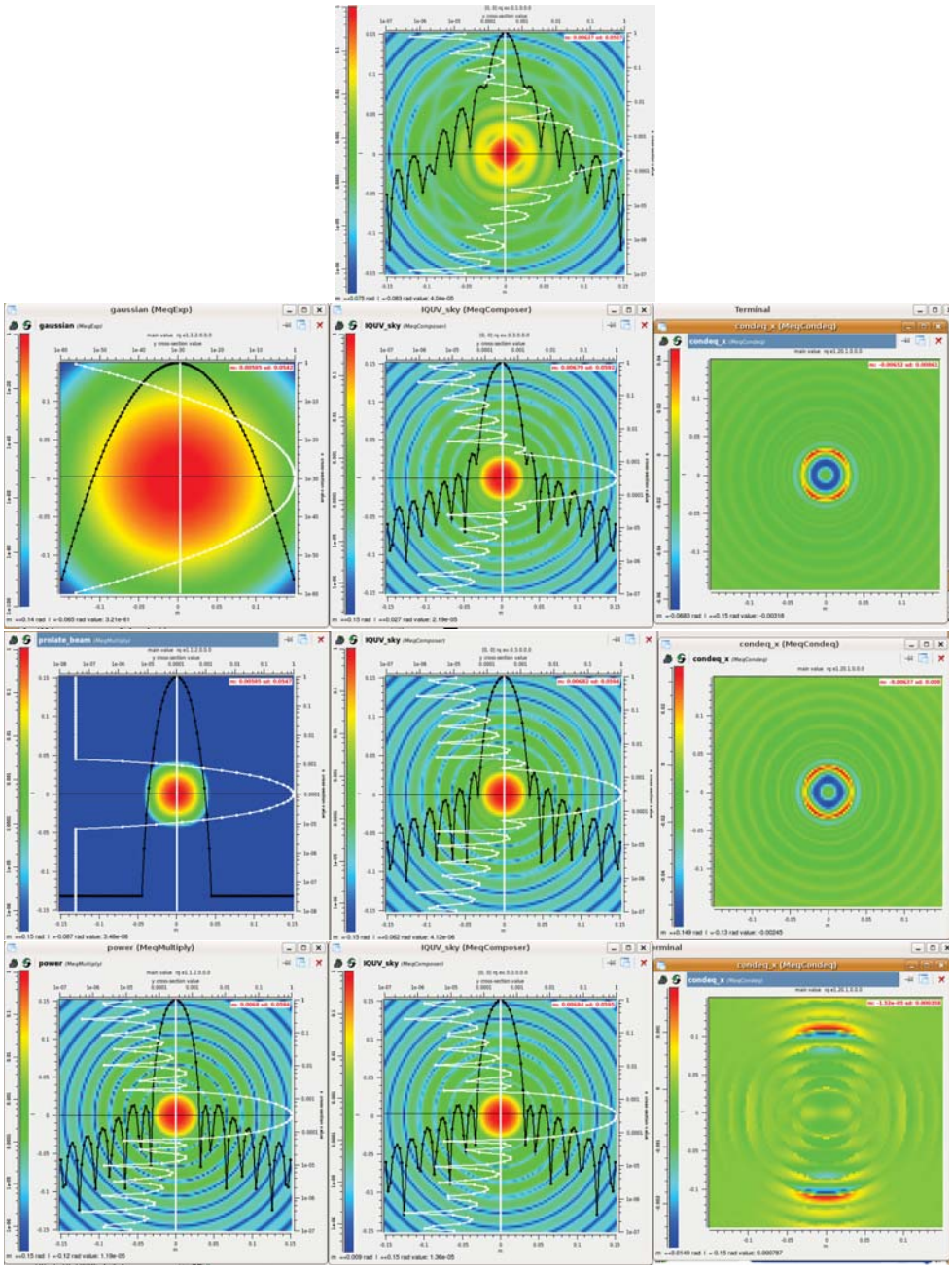


Figure 4: The top of this figure shows a phased-up beam centred on boresight with phase-conjugate weights. The three rows show the results of adjusting the weights by fitting to more desirable patterns - in order from top to bottom these are a Gaussian, prolate spheroid, and GRASP-designed pattern. The left column shows the target mathematical function or antenna power pattern. The central column shows the resulting phased up antenna power pattern. The right column shows the difference between the target and fitted voltage patterns for the X co-polarization fits. (A perfect fit would give a value of zero everywhere.) The target and fitted antenna power patterns are shown with a logarithmic scale, while the differences are shown with a linear scale. The fit to the GRASP design is clearly superior to the other fits.

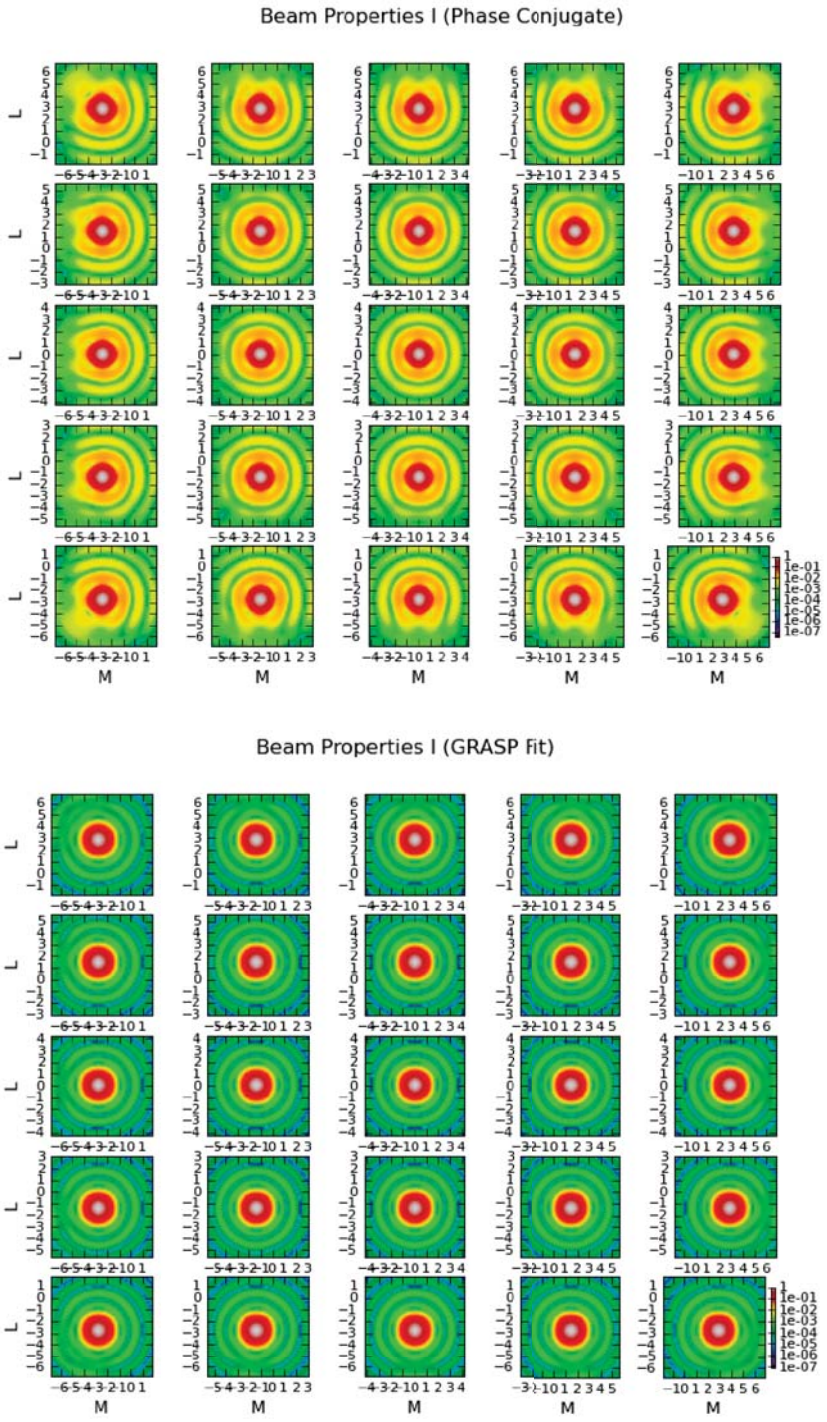


Figure 5: Phased up Stokes I total intensity responses obtained using phase-conjugate weighting (top figure) and the corresponding beam shapes obtained from the GRASP-target fit procedure (bottom figure).These beams are displayed with a logarithmic scale and the coordinates are given in degrees.

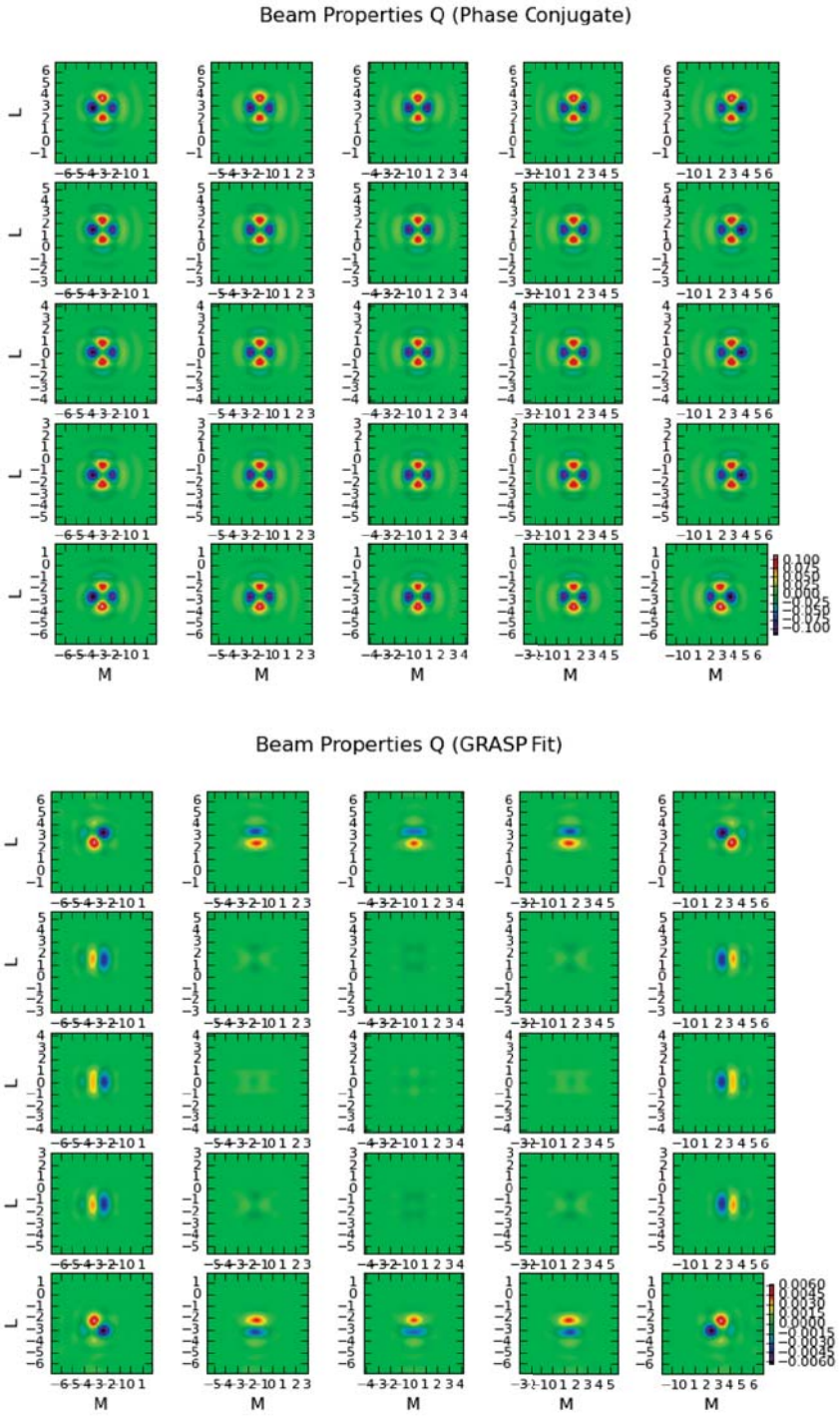


Figure 6: Phased up Stokes Q instrumental polarization responses obtained using phase-conjugate weighting (top figure) and the corresponding beam shapes obtained from the GRASP-target fit procedure (bottom figure). The responses are displayed with a linear scale.

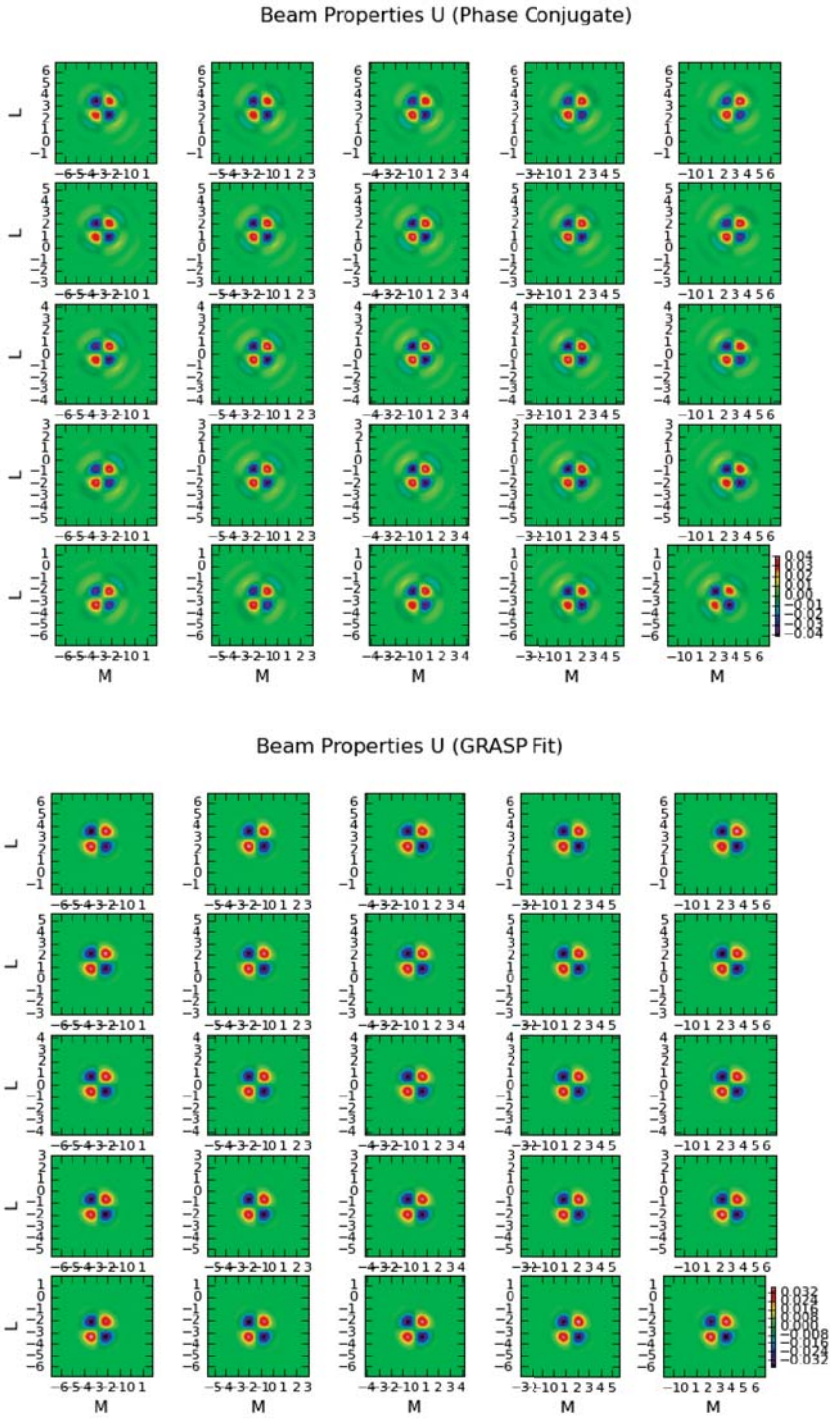


Figure 7: Phased up Stokes U instrumental polarization responses obtained using phase-conjugate weighting (top figure) and the corresponding beam shapes obtained from the GRASP-target fit procedure (bottom figure). The responses are displayed with a linear scale.

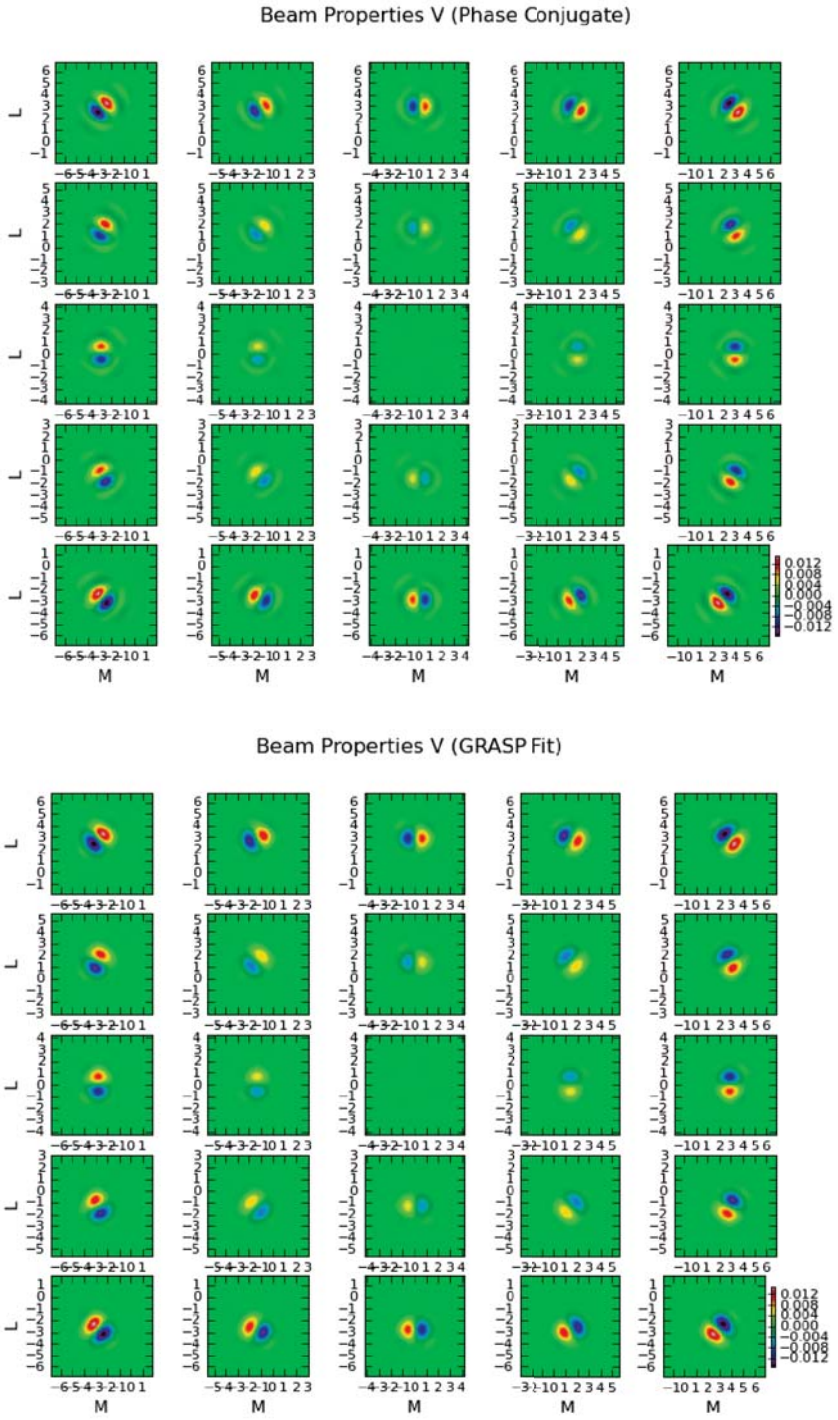


Figure 8: Phased up Stokes V instrumental polarization responses obtained using phase-conjugate weighting (top figure) and the corresponding beam shapes obtained from the GRASP-target fit procedure (bottom figure). The responses are displayed with a linear scale.

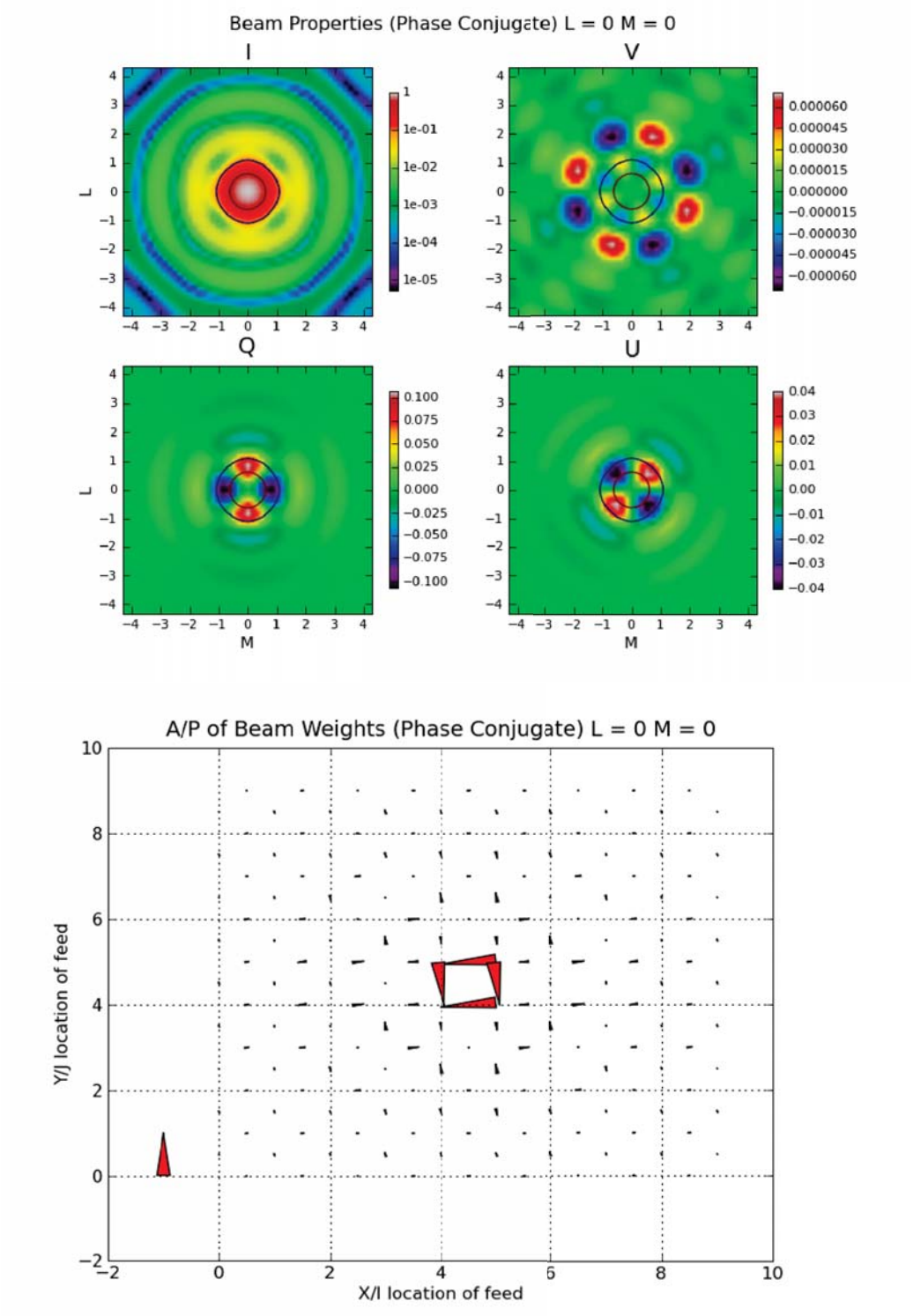


Figure 9: The phased-up beam obtained at boresight using phase-conjugate weighting (top figure) and the corresponding distribution of weights (bottom figure). In the top figure, the units of L and M are now given in degrees. In this and following figures contours are shown at the 10% and 50% response level of the Stokes I beam.

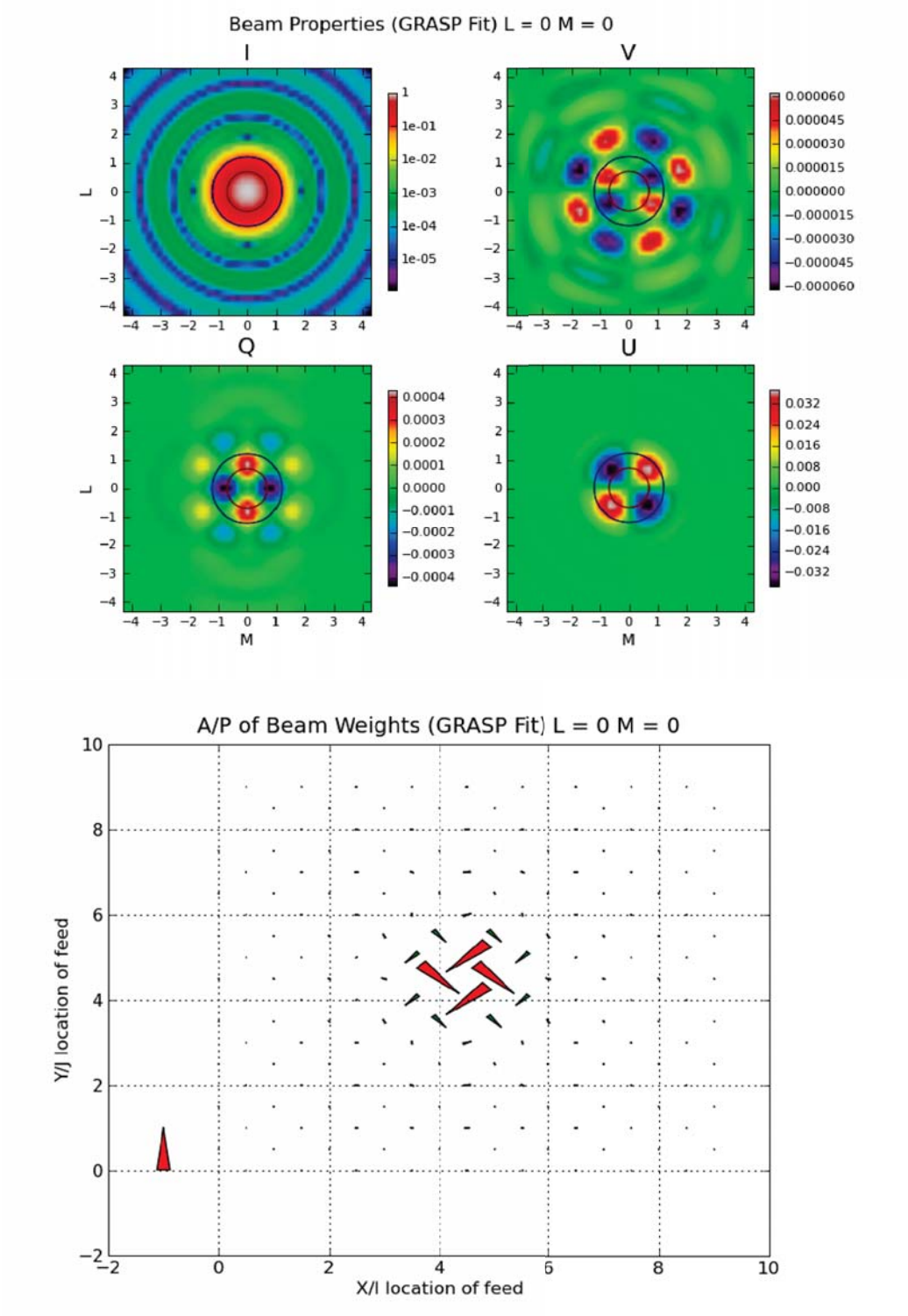


Figure 10: The phased-up beam obtained at boresight using a GRASP-target fit (top figure) and the corresponding distribution of weights (bottom figure).

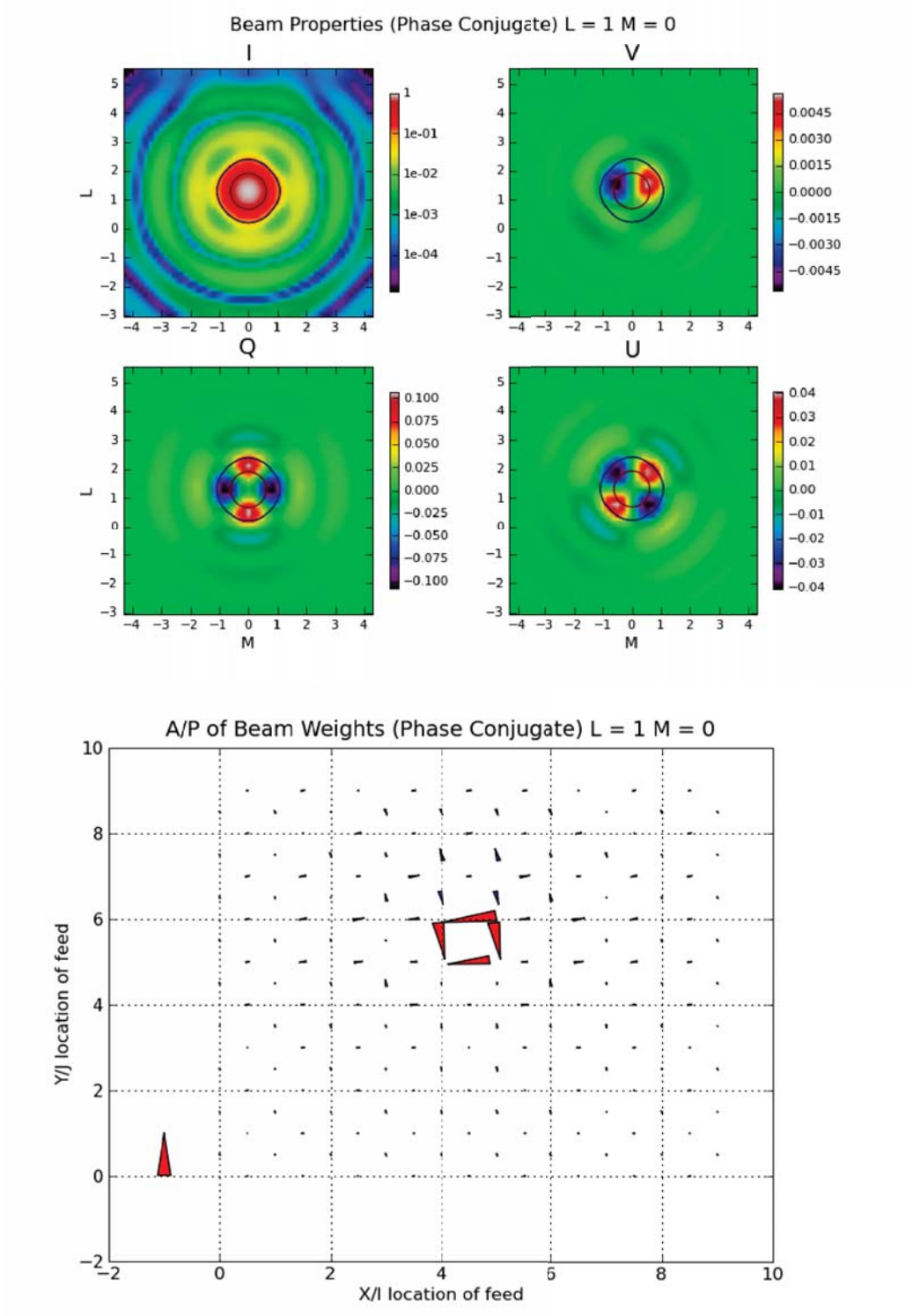


Figure 11: The phased-up beam obtained at L = 1 x FWHM, M = 0 using phase-conjugate weighting (top figure) and the corresponding distribution of weights (bottom figure).

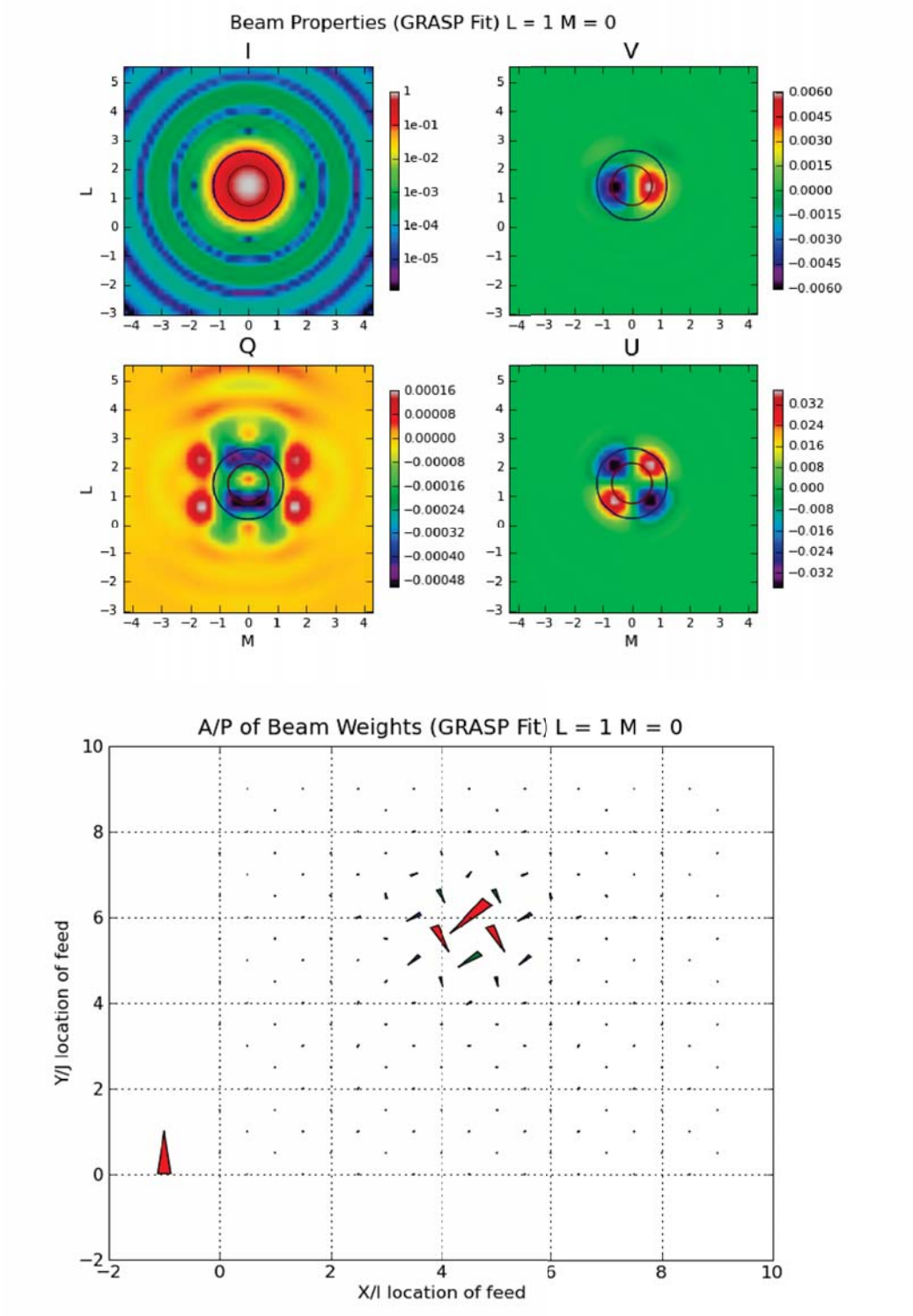


Figure 12: The phased-up beam obtained at L = 1 x FWHM, M = 0 using a GRASP-target fit (top figure) and the corresponding distribution of weights (bottom figure).

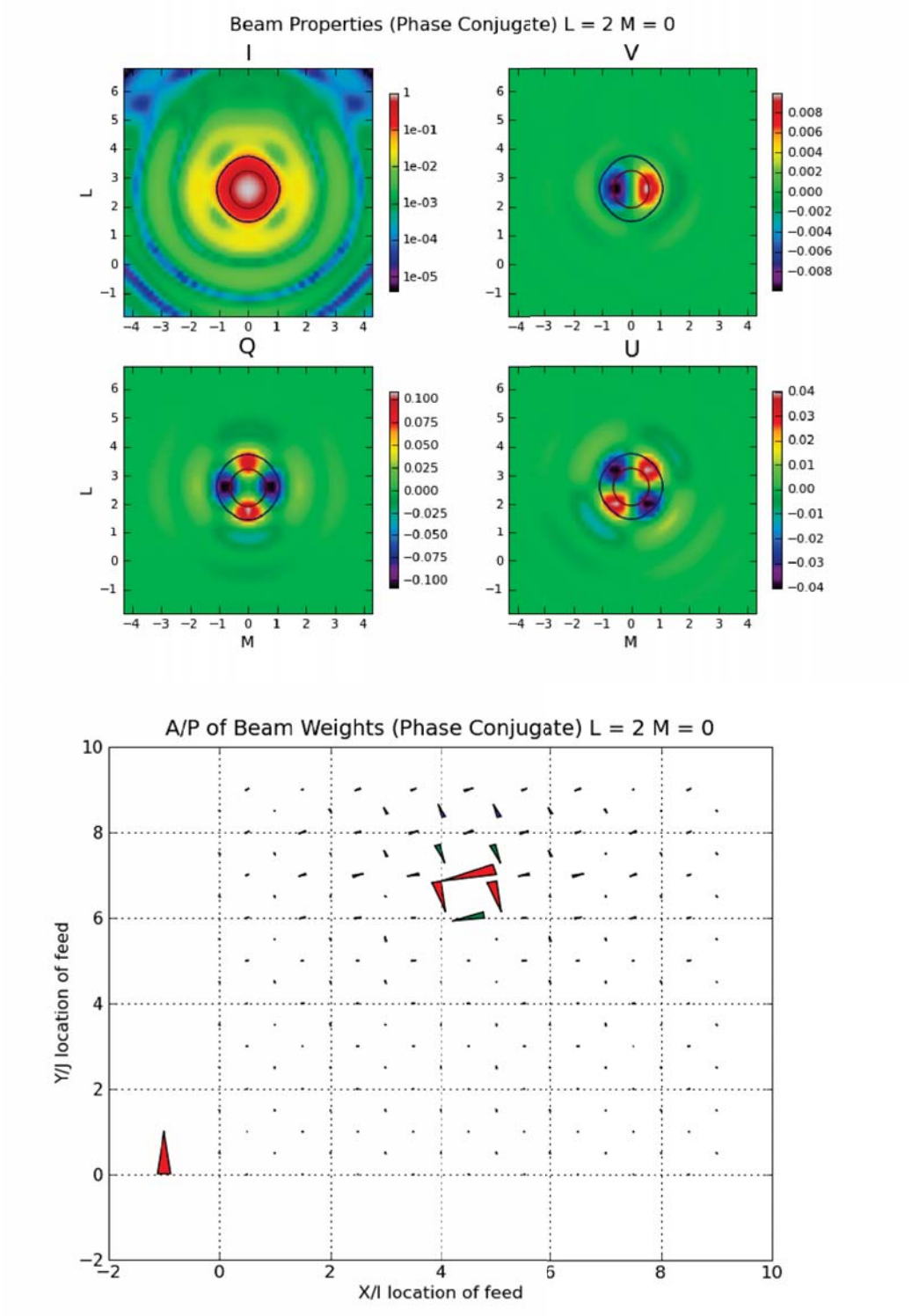


Figure 13: The phased-up beam obtained at L = 2 x FWHM, M = 0 using phase-conjugate weighting (top figure) and the corresponding distribution of weights (bottom figure).

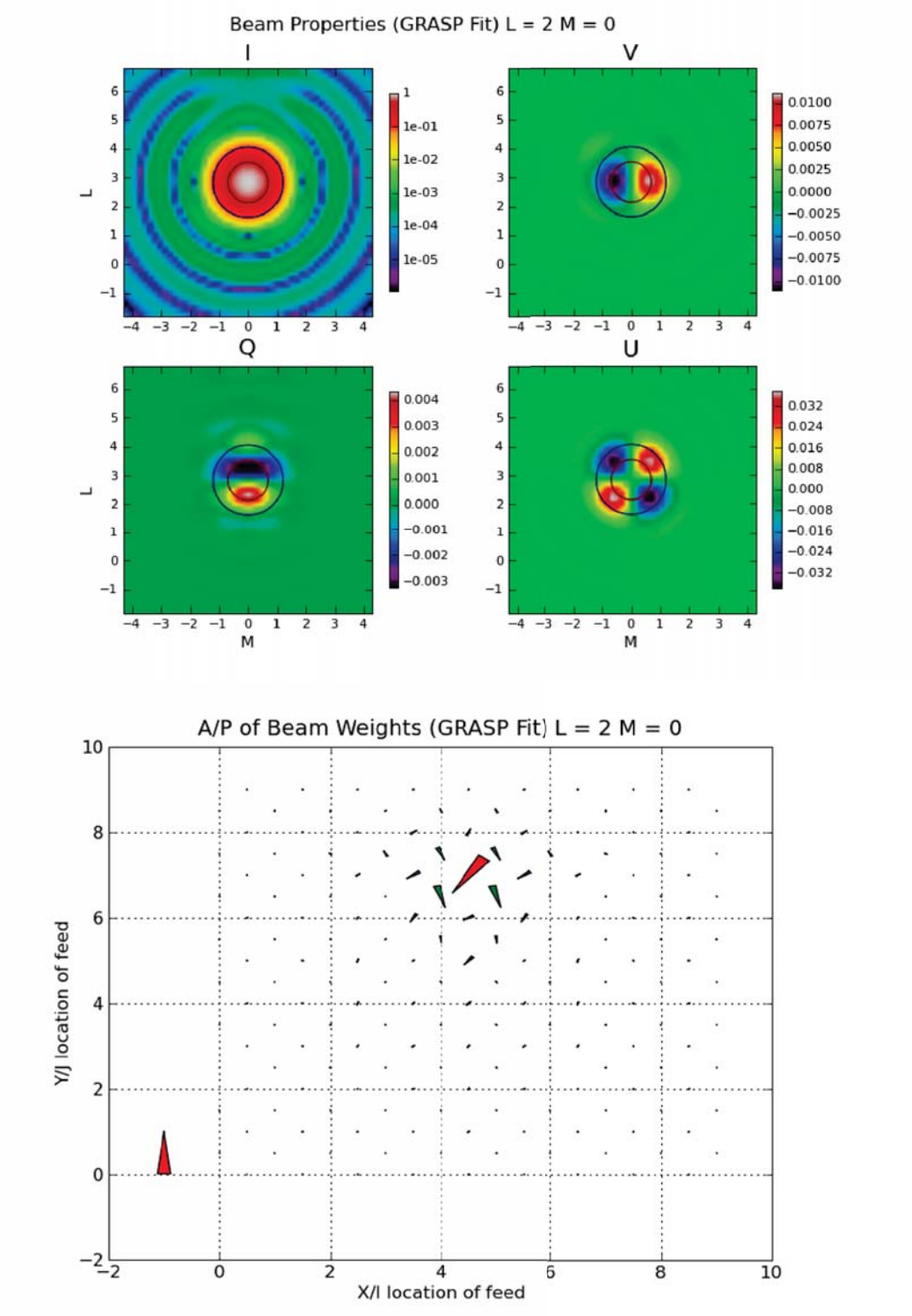


Figure 14: The phased-up beam obtained at L = 2 x FWHM, M = 0 using a GRASP-target fit (top figure) and the corresponding distribution of weights (bottom figure).

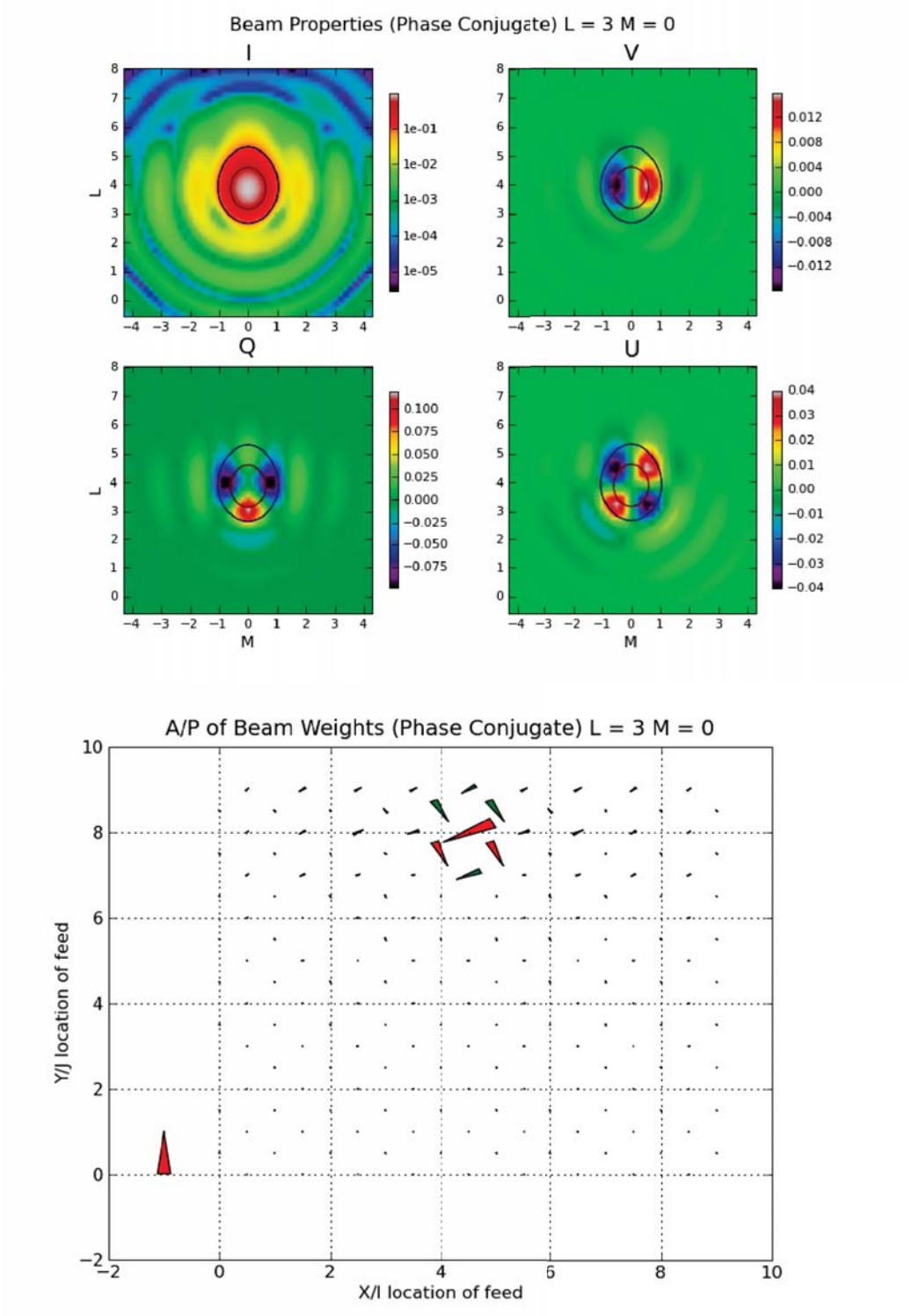


Figure 15: The phased-up beam obtained at L = 3 x FWHM, M = 0 using phase-conjugate weighting (top figure) and the corresponding distribution of weights (bottom figure).

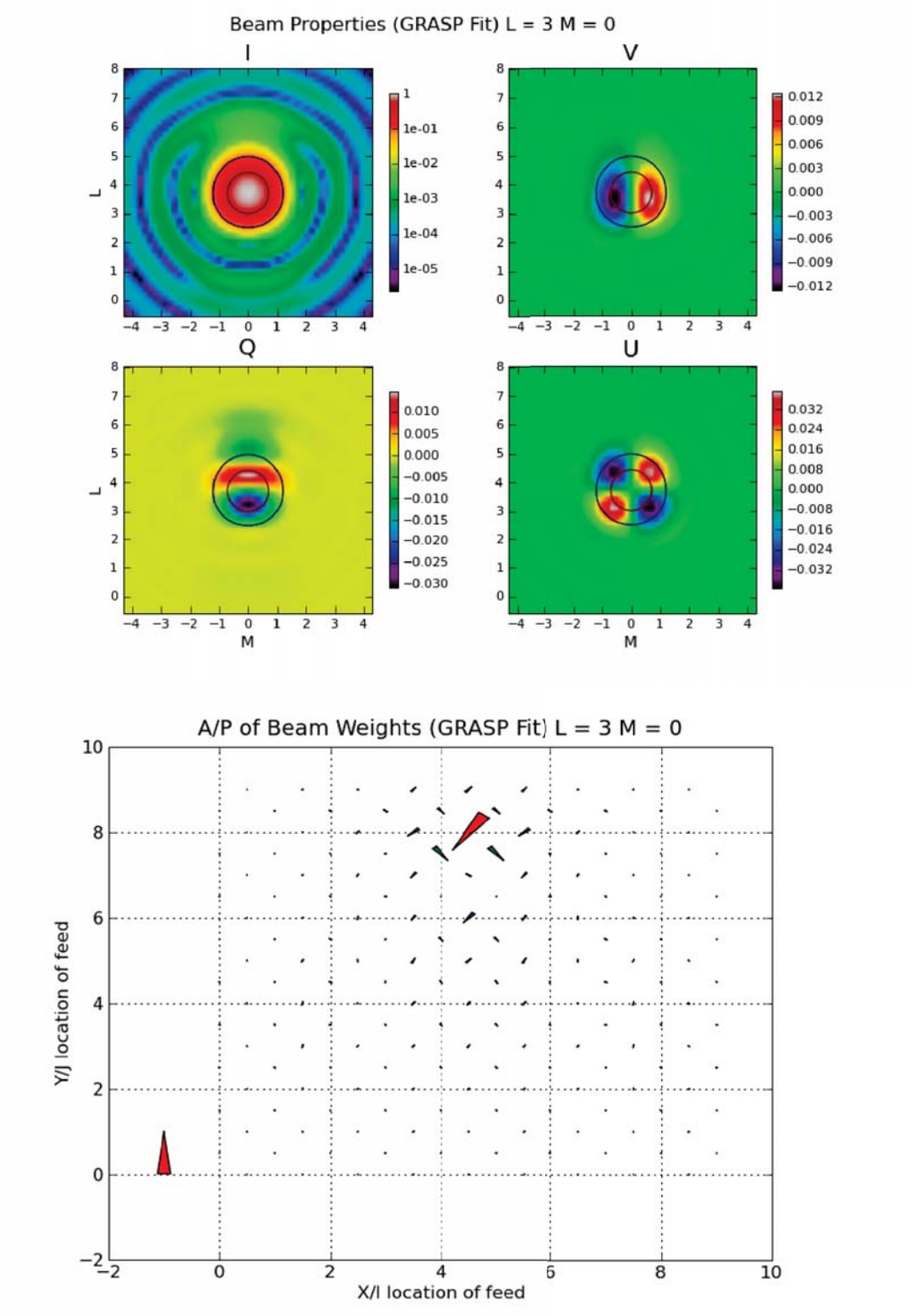


Figure 16: The phased-up beam obtained at L = 3 x FWHM, M = 0 using a GRASP-target fit (top figure) and the corresponding distribution of weights (bottom figure).

[3] R. T. Schilizzi, "The Square Kilometre Array," *Proc. SPIE (Ground Based Telescopes)*, 2004.

[4] E. Ohm, "Multifixed-Beam Satellite Antenna with Full Area Coverage and a Rain-Tolerant Polarization Distribution," *IEEE Trans. Antennas and Propagation*, vol. AP-29, pp. 937–943, 1981.

[5] L. Staveley-Smith, W. Wilson, T. Bird, M. Disney, R. Ekers, K. Freeman, R. Haynes, M. Sinclair, R. Vaile, R. Webster, and A. Wright, "The Parkes 21-cm Multibeam Receiver," *Publications of the Astronomical Society of Australia*, vol. 13, pp. 243–248, 1996. [Online]. Available: http://www.atnf.csiro.au/research/multibeam/papers/TheParkes21cmMultibeam.ps.gz

[6] R. Olsson, P-S. Kildal, and S. Weinreb, "The Eleven Antenna: A Compact Low-Profile Decade Bandwidth Dual Polarized Feed for Reflector Antennas," *IEEE Trans. Antennas and Propagation*, vol. 54, no. 2, pp. 368–375, 2006. [Online]. Available: http://ieeexplore.ieee.org/xpls/abs_all.jsp?arnumber=1589404

[7] H. Holter, T.-H. Chio, and D. H. Schaubert, "Experimental Results of 144-Element Dual-Polarized Endfire Tapered-Slot Phased Arrays," *IEEE Trans. Microwave Theory and Techniques*, vol. 48, no. 11, pp. 1707–1718, Nov. 2000. [Online]. Available: http://ieeexplore.ieee.org/xpls/abs_all.jsp?arnumber=900228

[8] P. J. Gibson, "The Vivaldi Aerial," in *9th European Microwave Conference*, 1979, pp. 101–105.

[9] B. M. Gaensler, R. Beck, and L. Feretti, "The Origin and Evolution of Cosmic Magnetism," in *Science with the Square Kilometre Array*, 2004. [Online]. Available: http://www.skatelescope.org/pages/page_sciencegen.htm

[10] A. R. Taylor, J. M. Stil, J. K. Grant, T. L. Landecker, R. Kothes, R. I. Reid, A. D. Gray, D. Scott, P. G. Martin, A. I. Boothroyd, G. Joncas, F. J. Lockman, J. English, A. Sajina, and J. R. Bond, "Radio Polarimetry of the elais n1 Field: Polarized Compact Sources," *The Astrophysical Journal*, vol. 666, pp. 201–211, Sep. 2007.

[11] W. Brisken and C. Craeye, "Evla Memo 69: Focal Plane Array Beam-forming and Spill-over Cancellation using Vivaldi Antennas," NRAO, Tech. Rep., 2004. [Online]. Available: http://www.aoc.nrao.edu/evla/memolist.shtml

[12] B. Veidt, T. Burgess, R. Messing, G. Hovey, and R. Smegal, "The drao phased array feed demonstrator: Recent results," in *"Antenna Technology and Applied Electromagnetics and the Canadian Radio Science Meeting, 2009. ANTEM/URSI 2009. 13th International Symposium"*, Feb. 2009.

[13] W. van Cappellen and L. Bakker, "Initial results of the digital focal plane array demonstrator for Apertif," 2008, deep Surveys of the Radio Universe with SKA Pathfinders, Perth, 31 March – 4 April 2008. [Online]. Available: http://ska2008.ivec.org/SKA_Pathfinder-talks-posters.htm

[14] M. Ivashina, "Dutch Fpa progress – Characterization of Efficiency, System Noise Temperature and Sensitivity of Focal Plane Arrays," 2008, deep Surveys of the Radio Universe with SKA Pathfinders, Perth, 31 March – 4 April 2008. [Online]. Available: http://ska2008.ivec.org/SKA_Pathfinder-talks-posters.htm

[15] K. F. Warnick *et al.*, "BYU/NRAO 2007 Green Bank 20 Meter Focal Plane Array – Modeling and Experimental Results," 2007, SKADS MCCT Technical Workshop 'Design of Wideband Receiving Array Systems' SKADS Marie Curie workshop, 26–30 November 2007. [Online]. Available: http://www.astron.nl/workshop/MCCT/program_fi.htm

[16] J. P. Hamaker, J. D. Bregman, and R. J. Sault, "Understanding radio polarimetry. i. Mathematical Foundations," *Astron. Astrophys. Suppl. Series*, vol. 117, pp. 137–147, 1996.

[17] J. E. Noordam, "The Measurement Equation of a Generic Radio Telescope - Aips++ Implementation Note nr 185," ASTRON, Tech. Rep., 1996. [Online]. Available: http://www.astron.nl/ noordam/

[18] O. M. Smirnov, "Meqtree workshop 2007," ASTRON, Tech. Rep., 2007. [Online]. Available: http://www.astron.nl/meqwiki/MeqTreeWorkshop2007

[19] J. P. Hamaker, "Understanding radio polarimetry. iv. The full-coherency analogue of scalar self-calibration: Self-alignment, dynamic range and polarimetic fidelity," *Astron. Astrophys. Suppl. Series*, vol. 143, pp. 515–534, 2000.

[20] P. Napier, "The Primary Antenna Elements," *ASP Conference Series*, vol. 180, pp. 37–56, 1999.

[21] W. Cotton, "Polarization in Interferometry," *ASP Conference Series*, vol. 180, pp. 111–126, 1999.

[22] K. Pontoppidan, "Grasp9: Technical description," TICRA Engineering Consultants, Tech. Rep., 2005.

[23] J. E. Noordam and O. M. Smirnov, "Meqtrees: A software module for implementing an arbitrary Measurement Equation and solving for its parameters," *In Preparation*, 2009.